Biochimica et Biophysica Acta 1828 (2013) 944–955

Contents lists available at SciVerse ScienceDirect

Biochimica et Biophysica Acta

journal homepage: www.elsevier.com/locate/bbamem

Design and characterization of novel antimicrobial peptides, R-BP100 and RW-BP100, with activity against Gram-negative and Gram-positive bacteria

Inês M. Torcato [a], Yen-Hua Huang [b], Henri G. Franquelim [a], Diana Gaspar [a], David J. Craik [b], Miguel A.R.B. Castanho [a], Sónia Troeira Henriques [a,b,*]

[a] Instituto de Medicina Molecular, Faculdade de Medicina, Universidade de Lisboa, 1649-028 Lisbon, Portugal
[b] Institute for Molecular Bioscience, The University of Queensland, Brisbane, QLD 4072, Australia

ARTICLE INFO

Article history:
Received 26 August 2012
Received in revised form 29 November 2012
Accepted 4 December 2012
Available online 13 December 2012

Keywords:
Antimicrobial peptide
Model membrane
Peptide–membrane interaction
Atomic force microscopy
Trp/Tyr fluorescence

ABSTRACT

BP100 is a short cationic antimicrobial peptide with a mechanism of action dependent on peptide–lipid interactions and microbial surface charge neutralization. Although active against Gram-negative bacteria, BP100 is inactive against Gram-positive bacteria. In this study we report two newly designed BP100 analogues, RW-BP100 and R-BP100 that have the Tyr residue replaced with a Trp and/or the Lys residues replaced with an Arg. The new analogues in addition to being active against Gram-negative bacteria, possess activity against all tested Gram-positive bacteria. Mechanistic studies using atomic force microscopy, surface plasmon resonance and fluorescence methodologies reveal that the antibacterial efficiency follows the affinity for bacterial membrane. The studies suggest that the activity of BP100 and its analogues against Gram-negative bacteria is mainly driven by electrostatic interactions with the lipopolysaccharide layer and is followed by binding to and disruption of the inner membrane, whereas activity against Gram-positive bacteria, in addition to electrostatic attraction to the exposed lipoteichoic acids, requires an ability to more deeply insert in the membrane environment, which is favoured with Arg residues and is facilitated in the presence of a Trp residue. Knowledge on the mechanism of action of these antimicrobial peptides provides information that assists in the design of antimicrobials with higher efficacy and broader spectra of action, but also on the design of peptides with higher specificity if required.

1. Introduction

Polycationic antimicrobial peptides (AMPs) are present in virtually all organisms as part of the innate immune system and act as endogenous antibiotics. These peptides induce the direct destruction of a wide diversity of microorganisms [1–4]. Owing to their ability to attack different microorganisms, including bacteria, viruses and fungi, together with the growing problem of resistance to conventional antibiotics, AMPs have been regarded as promising candidates for the development of novel antibiotics [1–4]. The fact that microorganisms are less efficient in developing effective resistance mechanisms against AMPs than against classical antibiotics [1,3,5,6] further supports the use of AMPs as novel therapeutics. In addition, AMPs can act synergistically with conventional antibiotics [6]. Thus, even if not used on their own, AMPs can potentially be administered with classical antibiotics to improve their therapeutic activity.

Cationic AMPs are generally short and amphipathic and it has been proposed that they primarily interact with bacteria by binding to the microbial negatively-charged membrane [7–9]. Membrane targeting is followed by permeabilization leading to the disruption of the bacterial membrane structure [10,11]. Alternatively, some AMPs seem to cross the membrane without destroying it [11,12] and exert their activity through interaction with intracellular targets (e.g. binding to and inhibition of nucleic acids) [13]. Their preference for the more negatively-charged bacterial membranes over the eukaryotic membranes, which have an outer lipid leaflet globally neutral, can be responsible for their selectivity [6,11].

Although having potential applications, naturally occurring AMPs are susceptible to protease degradation and have low bioavailability. In an effort to overcome these disadvantages, peptides with shorter and improved amino acid sequences and, therefore, with increased

Abbreviations: H-bond, hydrogen bond; AMP, antimicrobial peptide; AFM, atomic force microscopy; RP-HPLC, reversed phase high-performance liquid chromatography; MBC, minimal bactericidal concentration; MIC, minimal inhibitory concentration; *E. coli*, *Escherichia coli*; *S. aureus*, *Staphylococcus aureus*; *K. pneumoniae*, *Klebsiella pneumonia*; *P. aeroginosa*, *Pseudomonas aeroginosa*; *S. pneumonia*, *Streptococcus pneumonia*; *E. faecium*, *Enterococcus faecium*; ATCC, American type culture collection; MHB, Mueller Hinton broth; OD, optical density; PBS, phosphate buffered saline; NaCl, sodium chloride; S_{rms}, bacterial shape; R_{rms}, cell surface roughness; RBC, red blood cell; HC_{50}, peptide concentration needed to achieve 50% of haemolysis; IC_{50}, peptide concentration needed to achieve 50% of cell death; REES, red-edge excitation shift; HEPES, 4-(2-hydroxyethyl)-1-piperazineethanesulfonic acid; LUV, large unilamellar vesicles; POPC, 1-palmitoyl-2-Oleoyl-*sn*-Glycero-3-Phosphocholine; POPG, 1-palmitoyl-2-Oleoyl-*sn*-Glycero-3-Phosphoglycerol; 5/16-NS, 5/16- doxyl stearic acid; CD, circular dichroism; di-8-ANEPPS, 4-[2-[6-(dioctylamino)-2-naphthalenyl]ethenyl]-1-(3-sulfopropyl); PBMC, peripheral blood mononuclear cell; CF, carboxyfluorescein; LC_{50}, peptide concentration needed to induce 50% of leakage; $T_{1/2}$, time necessary to achieve 50% of leakage; LPS, lipopolysaccharide; LTA, lipoteichoic acid

* Corresponding author at: Institute for Molecular Bioscience, The University of Queensland, Brisbane, QLD 4072, Australia. Tel.: +61 7 33462026; fax: +61 7 33462101.
E-mail address: s.henriques@imb.uq.edu.au (S. Troeira Henriques).

0005-2736/$ – see front matter © 2012 Elsevier B.V. All rights reserved.
http://dx.doi.org/10.1016/j.bbamem.2012.12.002

antimicrobial activity and decreased cytotoxicity have been designed and synthesized [2,4,11,14]. BP100 (KKLFKKILKYL-NH_2) is a successful example of a synthetic AMP. Obtained from a combinatorial chemistry approach based on a cecropin A-melittin hybrid, BP100 is potent against Gram-negative bacteria, possesses low cytotoxicity and has low susceptibility to protease K degradation [14].

BP100 binds to the anionic bacterial membrane and neutralizes it [15]. Its ability to efficiently disrupt anionic model membranes but not neutral model membranes, suggests that BP100 selectively disrupts bacteria over mammalian cells [15]. More recently, BP100 was also shown to be able to internalize into eukaryotic cells without disrupting them [16]. This finding holds great promise for the use of BP100 as a means to treat eukaryotic cells that are infected with bacteria.

Although BP100 has potential application against *Escherichia coli* (*E. coli*) [17] and other Gram-negative bacteria [14], it does not have significant activity against tested Gram-positive bacteria [17]. In theory, the efficiency of AMPs can be enhanced by further improving their affinity for anionic membranes. Nevertheless, neither the role of the membrane composition nor the structural features of peptides required for specificity are, as yet, fully understood and predicting antimicrobial or cytotoxic activity from a given amino acid sequence is difficult.

In the present study, based on previous studies showing that Arg and Trp residues enhance AMP activity [18,19], we propose the development of new BP100 analogues with putative improved membrane-binding properties: RW-BP100 (RRLFRRILRWL-NH_2) and R-BP100 (RRLFRRILRYL-NH_2) in which the Trp residue was replaced with a Tyr or/and the Lys residues were replaced with Arg. The antimicrobial efficiency of the newly designed peptides was tested against several Gram-negative and Gram-positive bacteria, including non-resistant and resistant strains. Their mechanism of action was evaluated by direct bacterial imaging with atomic force microscopy (AFM) and by biophysical studies with model membranes. Our results show that the newly designed peptides are not only active against Gram-negative bacteria but also against all tested Gram-positive bacteria. This study reveals that by replacing Lys with Arg it is possible to gain activity against Gram-positive bacteria; this finding is very important as it provides information for AMP design where a more specific or a broader activity is desired and also provides information on the differences in AMP action against Gram-positive and Gram-negative bacteria.

2. Materials and methods

2.1. Peptide synthesis

BP100, R-BP100 and RW-BP100 were synthesized using microwave-assisted solid phase using an automatic peptide synthesizer (CEM Liberty) following standard Fmoc chemistry on a 2-chlorotrityl resin. The deprotected peptide was cleaved using trifluoroacetic acid and purified by RP-HPLC. The synthetic peptides had ≥95% purity, as confirmed by analytical RP-HPLC. Peptide concentrations were determined by absorbance at 280 nm assuming $\varepsilon = 1.49\times10^3\ M^{-1}\ cm^{-1}$ for BP100 and R-BP100 and $\varepsilon = 5.50\times10^3\ M^{-1}\ cm^{-1}$ for RW-BP100. The overall hydrophobicity of the three peptides was compared using their RP-HPLC retention times [20]. Samples were run using a linear AB gradient (1% /min) at a flow rate of 0.3 mL/min on a 0.3 mL analytical column. Eluent A was 0.05% TFA (v/v) in water and eluent B was 90% acetonitrile (v/v) and 0.05% TFA (v/v) in water.

2.2. Antimicrobial susceptibility assay

The antimicrobial activity of BP100 and its analogues was examined by evaluation of the bacterial growth inhibition and bactericidal activity. A microtiter broth dilution method was employed [21]. Gram-negative *Escherichia coli* ATCC 25922, *E. coli* CGSC 5167, *Klebsiella pneumoniae* ATCC 13883, *K. penumoniae* ATCC 700603, *Pseudomonas aeroginosa* ATCC 10145, *P. aeroginosa* ATCC 27653 and Gram-positive *Staphylococcus aureus* ATCC 25923, *S. aureus* ATCC 33591, *Streptococcus pneumonia* ATCC 33400, *S. pneumonia* ATCC700677, *Enterococcus faecium* ATCC 35667 and *E. faecium* ATCC 51559 were tested. Briefly, bacterial suspensions (5×10^5 cells/mL) were incubated with two-fold dilutions of peptides (solubilized in sterile water) in 96-well non-binding surface plates (NBS, corning) for 24 h at 37 °C and compared with antibiotics as controls (collestin for Gram-negative bacteria, and kanamycin or tetracycline against Gram-positive bacteria). The minimal inhibitory concentration (MIC) was the lowest concentration showing no visible growth. To confirm if the peptides were killing the bacteria, the minimal bactericidal concentration (MBC) was determined by adding 30 μL of resazurin dyes (0.01% (w/v)) to each well. The plates were incubated at 37 °C for further 18 h. Wells with blue colouration indicate dead microorganism, whereas wells with pink colouration indicate live microorganism. The MBC value is the lowest concentration of the wells with blue colouration. The assays were done with Mueller Hinton broth (MHB) and repeated four times.

2.3. Atomic force microscopy imaging

Direct observation of the effects induced by BP100, R-BP100 and RW-BP100 in the morphology of bacterial cells was obtained by AFM imaging as previously described [17]. Cell suspensions with 2×10^7 cells/mL were spun down at 13,000 rpm (8 min for *E. coli* and 30 min for *S. aureus*) and washed twice with 10 mM phosphate buffer solution (PBS) containing 150 mM NaCl, pH 7.4 to remove the media. The peptides were incubated with the bacteria and the slides prepared as before [17]. The final peptide concentrations were 1, 10 or 100 μM. On average, five individual bacterial cells from two different zones of each slide with a total area of $4\times4\ \mu m^2$ were imaged. Height, error and phase-shift images were recorded. Height images were treated with JPK data processing 4.0.23 and orthogonal projections were done in Gwyddion 2.24 (Czech Metrology Institute, Czech Republic). Cross sections on five bacterial cells were done using Gwyddion 2.24 to determine the average dimension of *E. coli* and *S. aureus* cells. The average dimensions of the non-treated bacterial cells are in agreement with previous observations [17,22,23] confirming the viability of the controls. *E. coli* and *S. aureus* cells had respectively 0.20 ± 0.01 μm and 0.40 ± 0.08 μm of height, 1.16 ± 0.07 μm and 1.06 ± 0.11 μm of width and 2.73 ± 0.58 μm and 1.66 ± 0.34 μm of length.

2.4. Bacterial surface roughness and swelling analysis of AFM images

The bacterial cell surface roughness (R_{rms}) was determined through root-mean-square calculations of flattened AFM height images as previously described [17]. Changes in bacterial shape (S_{rms}) were analysed following a protocol similar to the one used for roughness [17] but instead of using a flattened representation of the bacterial cell surface, a mean-filter treated AFM image of the general shape of the bacteria was used. With this treatment it was possible to remove the superficial bacterial roughness and analyse the general shape and volume of the bacteria. The S_{rms} was calculated using Eq. (1) [17]. Non-treated and peptide-treated bacteria were compared.

$$S_{rms} = \sqrt{\sum_{i=1}^{N} \frac{(Z_i - Z_m)^2}{(N-1)}} \quad (1)$$

2.5. Haemolytic assay

The haemolytic activity of the peptides was determined using human red blood cells (RBCs) as described before [24]. Briefly, peptides were solubilized in 10 mM HEPES buffer containing 150 mM NaCl, pH 7.4 and tested in triplicates (two-fold dilutions starting with 50 μM). Melittin, a peptide with known haemolytic properties was also included

as a positive control. Samples with HEPES buffer or 0.1% (v/v) Triton X-100 were used to establish 0% or 100% of haemolysis, respectively. The experiment was repeated three times. The peptide concentration needed to achieve 50% of haemolysis (HC_{50}) was determined as before [24].

2.6. Cytotoxicity against human cells

Cervical cancer cells (HELA) were cultured in T175 flasks at 37 °C in an atmosphere of 5% CO_2 with DMEM containing 10% FBS. Cells were seeded (5×10^3 cells/ well) in 96-well plate flat-bottomed plate for 24 h before assay. BP100 and its analogues were incubated for 2 h in concentrations ranging from 60 to 0.5 μM, final volume 100 μL in media without serum, to avoid degradation. Blank without peptide, and cells with Tx-100 were included to establish 0% and 100% of cell death. After incubation, peptides were washed with PBS, fresh media (100 μL) containing serum and 10 μL resazurin dye (0.02% (w/v)) were added to the cells and incubated for 18 h. Absorbance signal was monitored at 540 and 620 nm and the percentage of death cells was quantified by calculating the absorbance ratio, R, (R = A620/A540 nm) and considering 100% of cell death the R obtained with TX-100 and 0% of death the R obtained with cells without compound, using the equation:

$$\%\ Cell\ death = \frac{\left(R_{sample} - R_{blank}\right)}{\left(R_{TX-100} - R_{blank}\right)} \times 100 \quad (2)$$

2.7. Binding affinity for lipopolysaccharide and lipotheicoic acid

The endpoint Chromogenic Limulus Amebocyte Lysate (LAL) test kit (QLC-1000, Lonza) was employed to examine the ability of BP100 and its analogues to neutralize lipopolysaccharide (LPS) and lipoteichoic acid (LTA). This test is a sensitive indicator of the presence of free, non-neutralized endotoxin (either LPS or LTA) [25]. LPS from *E. coli* O111:B4 (standard provided with the LAL assay kit) or LTA from *S. aureus* (L2515 from Sigma) were incubated with various concentrations of BP100 and its analogues. Briefly, peptide and LPS (1 EU/mL), or LTA (500 ng/mL, response equivalent to LPS 1 EU/mL), were incubated for 30 min to allow binding. LAL reagent was added and incubated for 10 min at 37 °C, followed by addition of the colourless substrate and incubation for further 6 min as per manufacture instructions. The reaction was stopped with 25% (v/v) glacial acetic acid and the release of p-nitroaniline followed by absorbance at 405 nm. Controls with water or peptide only were included to confirm that all the samples were endotoxin-free. After blank subtraction, the concentration of free endotoxin was calculated by using calibration curves obtained with LPS (0.125–1 EU/mL) or LTA (62.5–1000 ng/mL). The values were normalized and converted into bound endotoxin (bound endotoxin = 1 − free endotoxin) and plotted as a function of peptide concentration. The experiment was repeated three times.

2.8. Preparation of lipid vesicles

Large unilamellar vesicles (LUVs) with a diameter of 100 nm, or small unilamellar vesicles (SUVs) with a diameter of 50 nm were used as membrane model and prepared by extrusion method as before [26]. LUVs were used in fluorescence studies whereas SUVs were used to prepare the bilayers for surface plasmon resonance studies [27]. Vesicles composed of 1-palmitoyl-2-oleoyl-*sn*-glycero-3-phosphocholine (POPC; Avanti Polar Lipids, USA) or with mixtures of POPC and 1-palmitoyl-2-oleoyl-*sn*-glycero-3-phosphoglycerol (POPG) were prepared for comparison. All the lipid systems were prepared in 10 mM HEPES buffer, pH 7.4 containing 150 mM NaCl.

2.9. Binding of BP100 and analogues with lipid bilayers followed by SPR

The ability of BP100 and its analogues to bind to phospholipid lipid bilayers was examined using SPR as described for other peptides [27]. L1 sensor chips and a Biacore 3000 instrument were used. The binding of the three peptides was compared for POPC, POPC/POPG (4:1 molar ratio) and POPC/POPG (1:1 molar ratio). Each measurement was repeated three times. The obtained sensorgrams were normalized for lipid deposition and peptide mass and represented as peptide-to-lipid ratio (P/L). The relative affinity was compared based on the P/L obtained at a reporting point at the end of the association phase (t = 170 s) [28].

2.10. Changes in membrane dipole potential

The membrane dipole potential can change upon insertion of peptide into the lipid membrane. Changes in model membranes dipolar potential were followed with fluorescence excitation spectra of the membrane dye (4-[2-[6-(dioctylamino)-2-naphthalenyl]ethenyl]-1-(3-sulfopropyl) (di-8-ANEPPS; Invitrogen, USA)) as before [27]. The dye (4 μM) was added to 200 μM POPC or POPC/POPG (1:1 molar) LUVs and incubated overnight. The fluorescence excitation spectra (λ_{em} = 613 nm for POPC and λ_{em} = 617 nm for POPC/POPG vesicles) were recorded before and after peptide addition (12.5, 25 and 50 μM, incubated for ~5 min).

Dipole potential variations in Human cells membrane were also monitored using RBCs and peripheral blood mononuclear cells (PBMCs) and the same peptide concentrations. Cell isolation and dye-labelling followed protocols previously described [29].

2.11. Vesicle aggregation

Vesicle aggregation induced by BP100, R-BP100 or RW-BP100 was followed by optical density at 436 nm (OD_{436}) [26]. The peptide (6.25, 12.5, 20, 25 and 50 μM) was added to POPC or POPC/POPG (4:1 or 1:1 molar) vesicles (500 μM final lipid concentration) and the OD followed as a function of time.

2.12. Vesicle leakage studies

Leakage of vesicle contents induced by BP100, R-BP100 and RW-BP100 was quantified by carboxyfluorescein (CF) fluorescence dequenching (lipid vesicles were prepared with 50 mM of CF solubilized in 10 mM HEPES buffer containing 150 mM NaCl). Vesicle preparation, lipid quantification and determination of leakage percentage followed protocols previously described [30]. Different peptide concentrations with two-fold dilutions starting from 100 μM were incubated with POPC or POPC/POPG (1:1 molar) LUVs (50 μM, final lipid concentration). The fluorescence intensity (λ_{exc} = 492 nm, λ_{em} = 518 nm) was measured after 5 min incubation and LC_{50} (peptide concentration needed to induce 50% of leakage) calculated as before [30]. The leakage kinetic was followed for 150 s after addition of peptide (25 μM) to POPC or POPC/POPG (1:1 molar) vesicles (50 μM lipid concentration) and the time necessary to achieve half of the response ($T_{1/2}$) was determined considering a pseudo-first order kinetic.

2.13. The fluorescence properties of BP100 and its analogues in aqueous solution and in membrane environment

The peptides included in this study have intrinsic fluorescence due to the presence of a Tyr (BP100 and R-BP100) or Trp residue (RW-BP100) in their sequence. Unless otherwise stated, BP100 and R-BP100 were excited at 274 nm and RW-BP100 was excited at 280 nm. Fluorescence emission spectra were scanned as a function of peptide concentration, pH and urea concentration. The existence of red-edge excitation shift effect (REES) was studied for RW-BP100: fluorescence emission spectrum was followed upon excitation with different wavelengths in the range

270 to 320 nm. Exposition of Tyr or Trp residue to the aqueous environment was evaluated by fluorescence emission quenching upon titration with acrylamide, as before [31]. To minimize the relative quencher/fluorophore light absorption ratio BP100 and R-BP100 were excited at 274 nm whereas RW-BP100 was excited at 290 nm. Fluorescence spectra with a band width of 5/10 nm for BP100 and R-BP100, or 3/6 nm for RW-BP100, were acquired at 25 °C in a spectrofluorimeter Edinburgh FS900 with 0.5 cm length quartz cuvettes. Peptides were solubilized in 10 mM HEPES buffer, pH 7.4 containing 150 mM NaCl.

To evaluate if the Trp or Tyr residue inserts in the lipid bilayer, the partition of BP100 and its analogues was followed by peptide fluorescence emission. Peptides were titrated with POPC or POPC/POPG (4:1 or 1:1 molar ratio) vesicle suspensions (final lipid concentrations in the range 0–4 mM). All the samples were incubated for five minutes before spectra scanning. To have negligible inner filter effect, the experiment was performed with 50 μM BP100 or R-BP100 and 15 μM of RW-BP100 (absorbance<0.1). The integrated area of each fluorescence spectrum was corrected for dilution and light dispersion, was normalized for the signal in buffer (I/I_W) and plotted as a function of lipid concentration [32]. The partition coefficient, K_p, and the ratio of the fluorescence emission obtained when all the peptide molecules are partitioned in the lipid (I_L) to the fluorescence intensity when all the peptide molecules are in water environment (I_W), I_L/I_W, were determined by fitting a non-linear equation as previously detailed [32].

2.14. Peptide in-depth location in lipidic membranes

The membrane in-depth location of the Trp or Tyr residue in the tested peptides was determined by a differential fluorescence quenching approach as previously described [33]. Briefly, quenching of peptide fluorescence emission was evaluated in the presence of quenchers (acrylamide, 5- and 16- doxyl stearic acid (5- and 16-NS)) that localize with different depths in the membrane [33]. 50 μM of BP100 and R-BP100 or 15 μM of RW-BP100 was incubated with 3 mM POPC or POPC/POPG (1:1) vesicles and titrated with increasing concentrations of acrylamide, 5- or 16-NS (Sigma-aldrich, USA) as detailed elsewhere for other peptides [31]. Data were analysed using the Stern–Volmer equation and quenching efficiency quantified with K_{SV} (Stern–Volmer constant) [31]. When a positive deviation to the Stern–Volmer representation was observed data were analysed as sphere-of-action quenching [34].

2.15. Secondary structure followed by circular dichroism (CD) spectroscopy

CD spectra were obtained on a Jasco J-815 instrument (Jasco Co, Tokyo, Japan) using a 1 mm path length cuvette. Briefly, spectra were collected from 195 to 260 nm at a speed of 50 nm/min. Peptide and lipid samples were prepared in 10 mM phosphate buffer with 150 mM NaF, pH 7.4. The CD signal of the peptides (50 μM) was recorded in the absence/presence of POPC or POPC/POPG (1:1) vesicles (peptide-to-lipid ratio was 1:9 molar or 1:19 molar depending on the signal intensity and vesicles dispersion contribution). To evaluate the effect of low pH and of a denaturizing agent in the peptides structure, the peptide CD signal was also evaluated at pH 2 and in the presence of 5 mM urea. Spectra were corrected by subtracting the appropriate blank (buffer, lipid in buffer, urea in buffer or buffer at pH 2) and converted to mean residue molar ellipticity. Spectra were smoothed using the noise reduction routines provided with the J-815 spectropolarimeter software (using Savitzky–Golay method). A quantitative analysis of the percentage of helicity was performed using three deconvolution software packages (SELCON3, CONTINLL and CDSSTR). No agreement was obtained between the three packages, and therefore a quantitative analysis was not included.

3. Results

3.1. Design of BP100 derivatives and their hydrophobic and basic properties

BP100 [14], like many other antimicrobial peptides (e.g. cecropins, magainins, cathelicidins and defensins) [35], kills bacteria through targeting membranes. The aim of the present study was to improve the activity of BP100 by modulating its membrane-binding properties and to gain more insights into the importance of basic and hydrophobic residues for antimicrobial efficacy and spectrum of action. Therefore, two new BP100 analogues, RW-BP100 and R-BP100 (Fig. 1), in which the Tyr residue is replaced with a Trp residue and/or the Lys residues were replaced with Arg residues, were designed. The global charge is +6 for the three peptides and the overall hydrophobicity, as measured with RP-HPLC retention times (36.6 min for BP100, 37.7 min for R-BP100 and 40.4 min RW-BP100), follows the order BP100<R-BP100<RW-BP100.

The putative membrane-binding affinity trend of the three peptides was estimated using the Wimley & White membrane interface hydrophobic scale [36]. Most hydrophobic scales focus on the membrane hydrophobic bulk phase [37], whereas the Wimley & White scale predicts the partition of the whole residue from water to the phospholipid membrane interfaces [38], which is particularly relevant to predict the ability of a peptide to target membranes. The membrane-binding partition as estimated by Wimley & White scale suggests the following trend: BP100<R-BP100<RW-BP100 (see Fig 1).

3.2. Newly designed AMPs have higher antimicrobial activity than BP100

The antimicrobial activities of BP100, R-BP100 and RW-BP100 were tested against Gram-negative and Gram-positive bacterial strains (Table 1). These bacteria have pathological interest and possess strains with antibiotic resistance and therefore they were chosen as models of

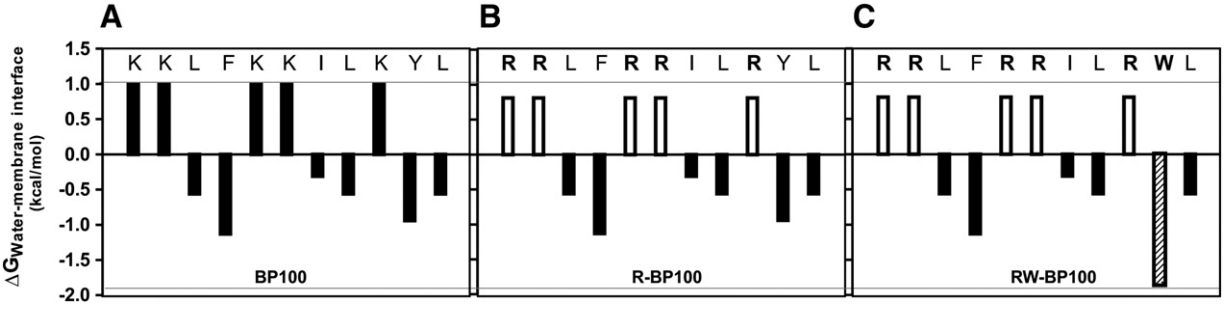

Fig. 1. Theoretical prediction of the affinity of the peptides for the membrane environment. The free transfer energy of (A) BP100, (B) R-BP100 and (C) RW-BP100 from water to POPC membranes interface ($\Delta G_{water-membrane\ interface}$) is represented based on Wimley & White amino acid interfacial hydrophobic scale [36]. Amino acids with $\Delta G_{water-membrane\ interface}<0$ have higher affinity for the membrane interface region than for the aqueous environment. The new derivatives, R-BP100 and RW-BP100, have the Lys residues mutated with Arg residues (white bars) and RW-BP100 also has the Tyr residue replaced with a Trp residue (shaded bar). The residues that were not mutated are represented with black bars.

Table 1
Antimicrobial activity of BP100, R-BP100 and RW-BP100.[a]

Bacterial strain and species	Relevant feature	MIC (μM)[b]			MBC (μM)[c]		
		BP100	R-BP100	RW-BP100	BP100	R-BP100	RW-BP100
Gram negative							
Escherichia coli ATCC 25922	control	2.0 ± 0.0	0.9 ± 0.4	0.5 ± 0.2	3.0 ± 0.6	1.1 ± 0.3	1.3 ± 0.3
Escherichia coli CGSC 5167	resistant, LPS mutant	0.7 ± 0.2	0.4 ± 0.1	0.2 ± 0.1	1.3 ± 0.5	0.5 ± 0.0	0.3 ± 0.1
Klebsiella pneumoniae ATCC 13883	control	1.0 ± 0.0	0.3 ± 0.2	0.1 ± 0.0	3.5 ± 0.5	0.4 ± 0.1	0.4 ± 0.1
Klebsiella pneumoniae ATCC 700603	multiresistant	4.0 ± 0.0	0.6 ± 0.3	0.3 ± 0.0	4.0 ± 0.0	2.1 ± 0.7	0.9 ± 0.1
Pseudomonas aeruginosa ATCC 10145	control	8.0 ± 0.0	2.0 ± 0.0	2.5 ± 0.5	8.0 ± 0.0	4.5 ± 1.3	3.5 ± 0.5
Pseudomonas aeruginosa ATCC 27853	resistant	4.0 ± 0.0	1.5 ± 0.3	1.5 ± 0.3	4.0 ± 0.0	1.5 ± 0.3	1.8 ± 0.3
Gram positive							
Staphylococcus aureus ATCC 25923	control	32.0 ± 0.0	6.0 ± 1.2	0.8 ± 0.1	32.0 ± 0.0	8.0 ± 0.0	1.0 ± 0.0
Staphylococcus aureus ATCC 33591	resistant	16.0 ± 0.0	3.0 ± 0.6	0.3 ± 0.1	28.0 ± 4.0	4.0 ± 0.0	0.6 ± 0.1
Streptococcus pneumoniae ATCC 33400	control	32.0 ± 0.0	5.0 ± 1.0	0.8 ± 0.1	32.0 ± 0.0	7.0 ± 1.0	1.0 ± 0.0
Streptococcus pneumoniae ATCC 700677	resistant	16.0 ± 0.0	4.0 ± 0.0	0.4 ± 0.1	28.0 ± 4.0	6.0 ± 1.2	0.9 ± 0.1
Enterococcus faecium ATCC 35667	control	32.0 ± 0.0	4.0 ± 0.0	1.0 ± 0.0	32.0 ± 0.0	4.0 ± 0.0	1.1 ± 0.3
Enterococcus faecium ATCC 51559	multiresistant	16.0 ± 0.0	2.0 ± 0.0	1.0 ± 0.0	16.0 ± 0.0	2.0 ± 0.0	1.0 ± 0.0

[a]The antimicrobial activity was determined in MHB. [b]MIC is the lowest concentration showing no visible growth. [c]MBC is the lowest concentration required to kill all the cells as measured with resazurin dye. The values shown are the average and standard error of four replicates.

Gram-negative and Gram-positive bacteria. Resistant and control strains were included for comparison. BP100 was active at low micromolar concentrations against all the Gram-negative bacteria tested (control and resistant strains) but has lower efficacy against Gram-positive bacteria, which is in agreement with previous reports [17,39]. The newly designed peptides were more active against Gram-negative bacteria than BP100, but most importantly are active at low micromolar concentration against all tested Gram-positive bacteria. RW-BP100 is the most active derivative, particularly against Gram-positive bacteria. It is worth noting that RW-BP100 has a MIC below 1 μM against tested resistant strains of *E. coli*, *S. aureus*, *K. pneumonia* and *S. pneumonia*. The determined MBC values are close to the MIC, revealing that the peptides are bactericidal and inhibit the bacterial growth by killing the bacteria.

Direct observation of the effects induced by BP100 and the two analogues was obtained by AFM imaging (Fig. 2). *E. coli* and *S. aureus* were used as models of Gram negative and Gram positive bacteria, respectively. BP100 and its analogues show identical effects on *E. coli* morphology. *E. coli* cells treated with 1 or 10 μM of peptide have their volume increased (Fig. 2E) and develop round-shaped structures on the membrane surface (Fig. 2A), which increase the overall surface roughness (Fig. 2C). When treated with 100 μM of BP100, or the analogues, the *E. coli* membrane is disrupted and the intracellular contents leak extensively (see Fig. 2A). These effects are in agreement with a previous report on BP100 [17].

Effects on *S. aureus* cell morphology, roughness and volume (Fig. 2B, D,F) were evident with R-BP100 and RW-BP100 at concentrations ≥10 μM, whereas BP100 only has visible effects at 100 μM. Membrane disruption of *S. aureus* is evident for all the peptides at the highest concentration tested.

3.3. Cytotoxicity and therapeutic index of BP100 and its analogues

The cytotoxicity of the peptides was assessed in HELA cells (Fig. 3A), revealing that BP100 is the least toxic peptide and RW-BP100 is the most toxic. Although being the most cytotoxic peptide, RW-BP100 has the highest therapeutic index (TI, i.e., the ratio of toxic dose to therapeutic dose (IC_{50}/MIC)) against Gram positive bacteria, whereas BP100 has the lowest TI (e.g. the TI of BP100, R-BP100 and RW-BP100 against the resistant *S. aureus* strain ATTC 33591 is 3, 6 and 48, respectively). When comparing the TI for Gram negative bacteria the three peptides have a therapeutic index ≥10 for all the resistant bacteria strains tested.

Haemolytic studies were also carried and showed that RW-BP100 is the most haemolytic peptide whereas BP100 has low haemolytic activity in the concentration range tested (see HC_{50} in Fig. 3B).

3.4. Binding to LPS and LTA

The outer membranes of Gram-positive and Gram-negative bacteria differ significantly in their composition, which could explain the selectivity of BP100 towards Gram-negative bacteria. In addition to a thicker peptidoglycan layer, Gram-positive bacteria have LTA exposed in the outer membrane, whereas Gram negative bacteria have a thin peptidoglycan layer and an outer lipid bilayer covered with LPS [40]. These negatively-charged molecules activate multiple signal transduction pathways and constitute the first physical barrier which needs to be transversed by antimicrobial peptides [41]. Therefore, the ability of BP100 and its analogues to bind to LPS and LTA was examined and compared using a LAL assay. Fig. 4 shows that the three peptides are able to bind and neutralize LPS and LTA, but BP100 has the weakest activity. R-BP100 and RW-BP100 have identical activity to neutralize both molecules.

3.5. BP100 and its analogues have preference for negatively-charged membranes as identified by SPR

The ability of BP100 and its analogues to bind to phospholipid bilayers was examined using SPR to gain insights into their mechanism of action (Fig. 5). Membranes composed of zwitterionic POPC, which mimics the bulk fluid phase in eukaryotic cell membranes, were compared with POPC/POPG mixtures to mimic anionic bacterial cell membranes. SPR studies confirmed that BP100 has the lowest affinity for the membrane whereas RW-BP100 has the highest affinity. The three peptides have a preference for more anionic membranes relative to zwitterionic membranes (Fig. 5C). The preference of BP100 for more anionic membranes in relation to neutral membranes is in agreement with a previous study [15]. As predicted using the Wimley & White amino acid hydrophobic scale (see Fig. 1), the new derivatives have higher affinity for membranes than BP100.

3.6. Changes in the dipolar potential induced by BP100 and its analogues

Changes in the membrane dipole potential might occur upon insertion of peptides into phospholipid bilayers and can be monitored through spectral shifts in the fluorescence excitation spectra of di-8-ANEPPS probe [42]. The three peptides induced a larger change in the dipolar potential of POPC/POPG (1:1) than in POPC membranes (Fig. 6A & B), confirming a preference for negatively-charged membranes in respect to zwitterionic membranes. In addition, changes in dipolar potential reveal that these peptide molecules are inserting in the anionic lipid membranes rather than just being adsorbed at the phospholipid headgroup

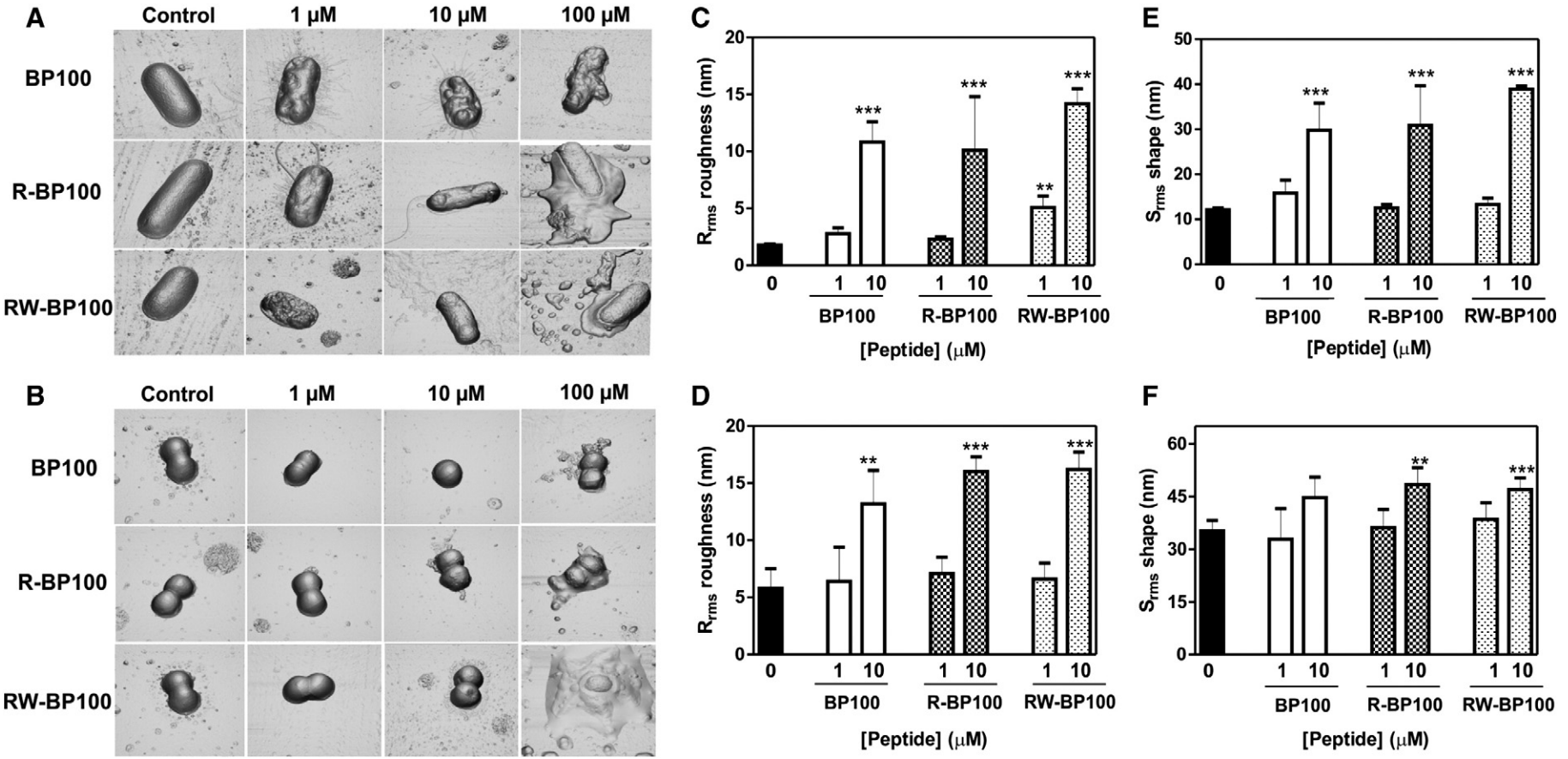

Fig. 2. The effect of BP100, R-BP100 and RW-BP100 on *E. coli* and *S. aureus* cells as monitored by AFM. (A, B) Orthogonal tridimensional projections of *E. coli* (A) and *S. aureus* (B) cells incubated for 2 h in the absence (control) or in the presence of 1, 10 or 100 μM of peptide. Images have a total area of $4 \times 4\ \mu m^2$. (C, D) Differences in the superficial roughness and (E, F) in bacterial shape of *E. coli* and *S. aureus* cells were determined through root-mean-square calculation (R_{rms} and S_{rms}, respectively). For each peptide concentration five bacterial cells were analysed. Asterisks represent the significance level of the difference between treated and non-treated bacterial cells. A one-way ANOVA and a Bonferroni test were employed. * $0.01 < p\text{-value} < 0.05$; ** $0.001 < p\text{-value} < 0.01$ and *** $p\text{-value} < 0.001$.

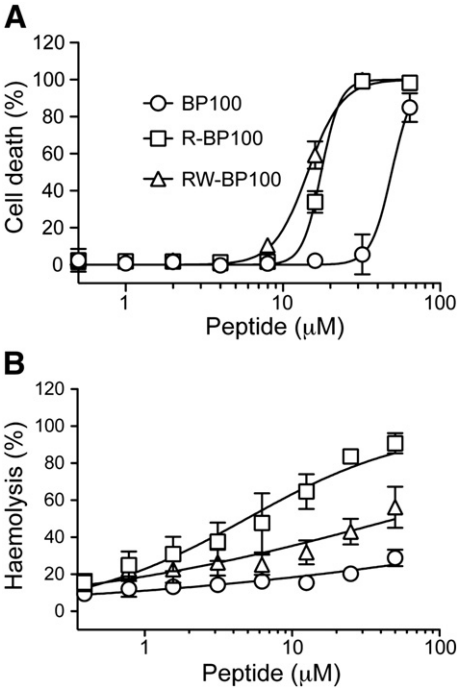

Fig. 3. Cytotoxicity and haemolytic activity of BP100 and its analogues. (A) Cytotoxicity dose response curves obtained against HELA cells as measured with a resazurin assay. Peptides were incubated with HELA cells for 2 h at 37 °C in medium without serum. The % of dead cells was determined by absorbance of the ratio of reduced/oxidized dye. The concentration needed to achieve 50% of cell death (IC_{50}) as obtained by a non-linear fit of the data was 49.2 ± 1.4, 17.5 ± 0.6 and 14.4 ± 0.4 μM for BP100, R-BP100 and RW-BP100, respectively. (B) Haemolysis dose response curves obtained after incubation of 0.25% (v/v) RBCs with peptide for 1 h at 37 °C; HC_{50} is >100 μM for BP100, 50.9 ± 25.0 μM for R-BP100 and 4.9 ± 1.0 μM for RW-BP100. Error bars represent standard error of the mean for three replicates.

region. RW-BP100 induced the largest change in the dipole potential in both lipidic mixtures studied (POPC and POPC/POPG 1:1). Significant alterations in the RBC's or PBMC's membrane dipole potential were not detected for any of the analogues (data not shown) at concentrations higher than the MIC (12.5, 25 and 50 μM), suggesting that these peptides do not insert significantly into human cells.

3.7. Vesicle aggregation and leakage induced by BP100 and its analogues

The membrane surfaces of vesicles can be brought in close proximity due to membrane–peptide–membrane interactions, resulting in vesicle aggregation [43]. The stability of vesicles dispersed in solution is mainly maintained by repulsive electrostatic forces and a repulsive hydration shell [43]. The interactions of positively-charged peptides with the negatively-charged membranes can cancel repulsive electrostatic forces and induce dehydration of the lipid polar groups. Such alterations make the surface more unstable and facilitate the aggregation of the vesicles [43]. The three peptides are able to induce aggregation of POPC/POPG (1:1) vesicles but not of the vesicles composed with POPC or POPC/POPG (4:1) (up to P/L = 0.1, Fig. 6C). These results support the finding that all three peptides prefer more negatively-charged membranes over neutral membranes and show that the membrane surface is disturbed upon peptide binding. BP100 showed the highest ability to induce aggregation of POPC/POPG (1:1 molar) vesicles at 25 μM, suggesting that this peptide more efficiently disturbs the membrane surface than the other two peptides. RW-BP100 showed the weakest vesicle surface destabilization ability.

It was previously reported that BP100 makes lipid vesicles permeable to Co^{2+} ions [15]. In the present study we evaluated the leakage of contents from POPC or POPC/POPG (1:1) vesicles induced by BP100 and its analogues (Fig. 6D and Table 2). Vesicles loaded with CF (final lipid concentration of 50 μM) were incubated with varying concentrations of peptide (up to P/L of two). BP100 and its analogues induce leakage of the anionic POPC/POPG (1:1) vesicles with identical efficiency (Table 2; LC_{50} ~ 5 μM, P/L ~ 0.1). RW-BP100 induces vesicle leakage at a faster rate than the other peptides, (see Fig. 6D and $T_{1/2}$ values in Table 2). A faster leakage rate might correlate with a faster membrane-binding rate.

Leakage from POPC vesicles occurs at a lower extension (Fig. 6D) and the efficiency is peptide dependent, being BP100 the least and RW-BP100 the most effective (Table 2). This trend is expected considering the haemolytic profile of the three peptides.

3.8. Fluorescence properties of BP100 and its analogues in buffer and in the presence of the lipid bilayer

BP100 and its analogues are intrinsically fluorescent due to Tyr or Trp residues in their sequence. The fluorescence of these aromatic residues is sensitive to its environment; therefore, the intrinsic steady-state fluorescence properties can give insights into the structure and organization of the peptides in the aqueous environment. BP100 and R-BP100 have excitation and emission spectra similar to L-Tyr amino acid ($\lambda_{excitation}$ maximum = 275 nm and $\lambda_{emission}$ maximum = 302 nm), whereas RW-BP100 has excitation and emission spectra identical to L-Trp amino acid in buffer ($\lambda_{excitation}$ = 280 nm and $\lambda_{emission}$ = 347 nm). These spectral characteristics suggest that BP100 and its analogues have the Tyr or Trp residue exposed to the solvent [44]. This finding is supported by the observation that the fluorescence quantum yield is independent of the peptide concentration (at least up to 100 μM) and independent of pH (as low as 2.5, data not shown). Due to the high sensitivity of Trp to the surrounding environment, the fluorescence of Trp-containing peptides might have REES as a result of peptide aggregation; this phenomenon is not so easily detected with Tyr fluorescence [44]. RW-BP100 fluorescence does not show REES, which supports a non-aggregated fluorophore

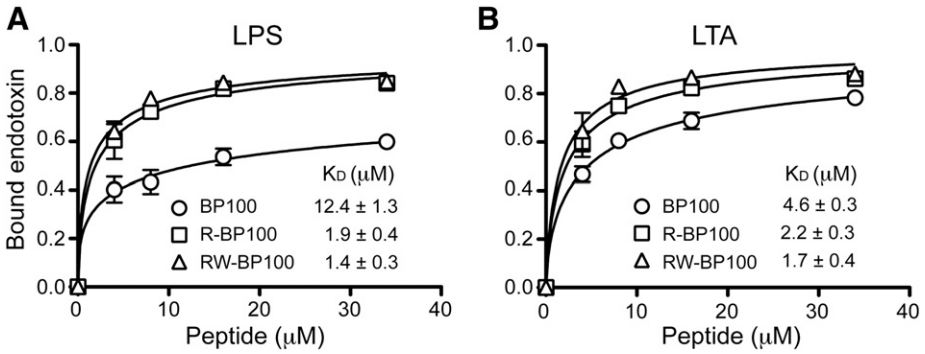

Fig. 4. Neutralization of LTA and LPS in the presence of BP100 or its analogues. Peptides were incubated with endotoxin for 30 min and the amount of free endotoxin quantified by LAL assay. The fraction of bound endotoxin as a function of peptide is shown. K_D is the peptide concentration required to neutralize 50% of endotoxin and was determined by non-linear fit of the data. Error bars represent standard error of the mean of three replicates.

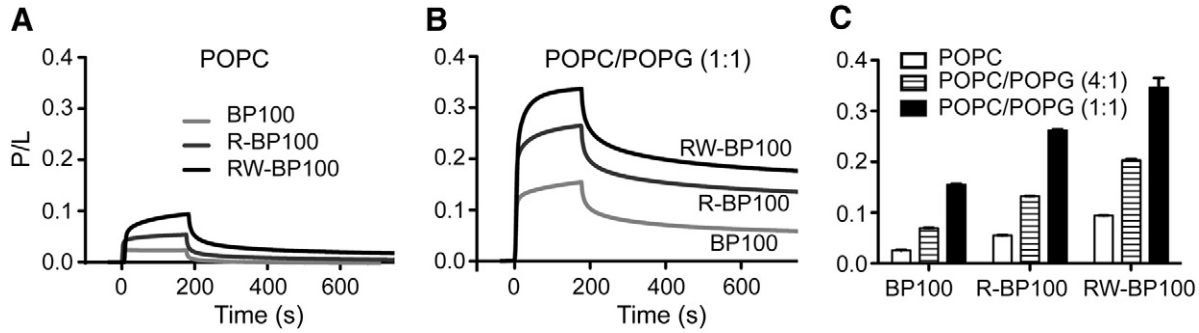

Fig. 5. Membrane-binding affinity of BP100 and its analogues as monitored by surface plasmon resonance. The response to the total amount of lipid deposited on the chip surface was normalized by calculating the peptide-to-lipid ratio (P/L mol/mol) (1RU = 1 pg·mm^{-2}). Sensorgrams obtained upon injection of 10 μM peptide over (A) POPC or (B) POPC/POPG (1:1) bilayers. (C) Comparison of the P/L obtained for the three peptides at a reporting point at the end of the association phase over POPC, POPC/POPG (4:1) or POPC/POPG (1:1) bilayers. Error bars represent standard error of the mean of three replicates.

population (data not shown). Overall, the fluorescence results suggest that BP100 and its analogues are non-structured and do not aggregate in aqueous solution.

The fluorescence emission quantum yield of the Tyr residue in BP100 or R-BP100 and of the Trp residue in RW-BP100 increased upon titration with lipid vesicles. In addition, RW-BP100 emission spectra have a blue shift characteristic of Trp residue transition from aqueous environment to a more hydrophobic environment [44]. Such alterations in the Tyr/Trp florescence suggest that these residues insert into the lipid bilayer. Therefore, the Tyr/Trp fluorescence emission can be used to quantify the relative affinity of these residues for lipid membranes through the determination of the partition coefficient, K_p [32]. In the three peptides the hydrophobic region binds with higher affinity to membranes with higher percentage of negatively-charged phospholipids, relative to zwitterionic membranes, as shown with K_p values (Table 3). In addition, at a fixed lipid concentration the fluorescence emission spectra of RW-BP100 have a larger blue-shift in POPC/POPG (1:1) relative to POPC membranes (e.g. 18 nm in 1 mM POPC/POPG (1:1) vs. 10 nm in 1 mM POPC). The trend observed for I_L/I_W (the ratio of the fluorescence emission obtained when all the fluorophores are partitioned in the lipid (I_L) to the fluorescence intensity when all the fluorophores are in water (I_W)) is BP100 ~ R-BP100 < RW-BP100 suggesting that RW-BP100 has its

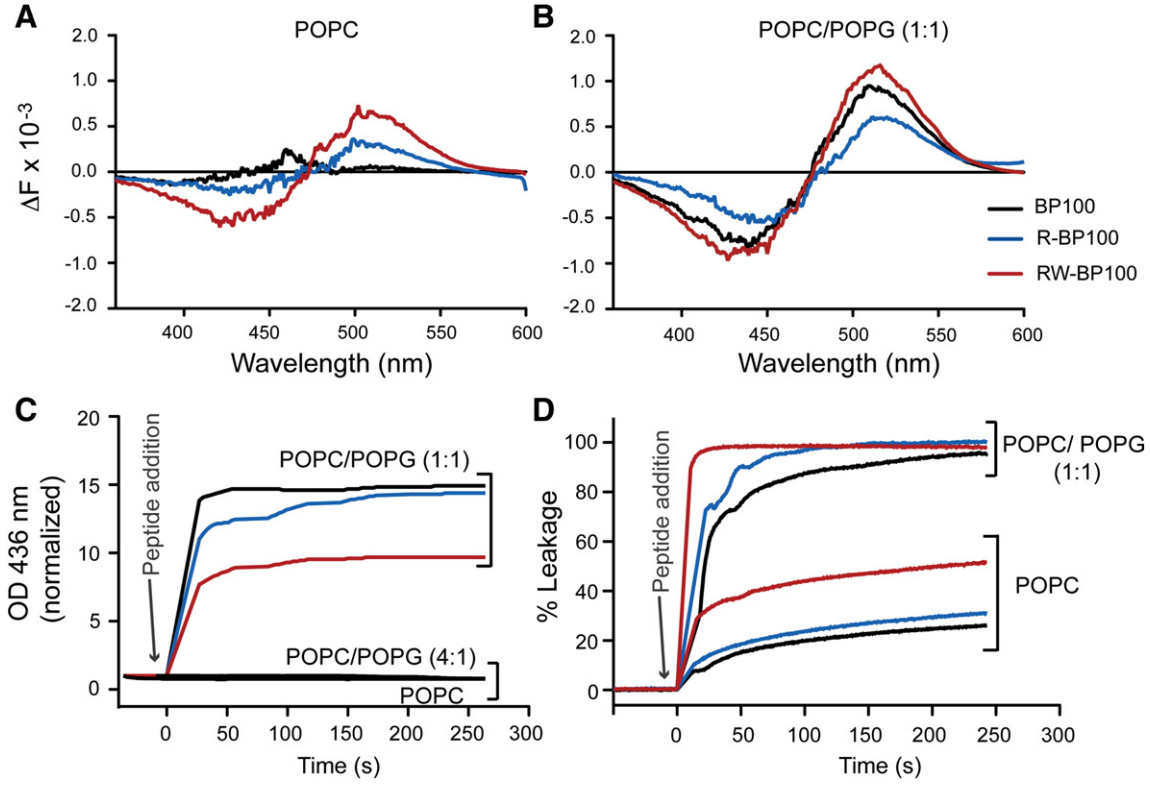

Fig. 6. Changes in membrane properties due to interaction with BP100 and its analogues. (A, B) Membrane dipole potential variation induced by 50 μM of BP100, R-BP100 or RW-BP100 in 200 μM of (A) POPC or (B) POPC/POPG (1:1 molar) vesicles. The final concentration of the di-8-ANNEPS probe was 4 μM. All the peptides induce a larger dipolar potential variation in POPC/POPG (1:1 molar) than in POPC vesicles. RW-BP100 induces the largest dipolar potential variation. (C) Vesicle aggregation studies. OD_{436nm} was monitored after addition of 25 μM of BP100, R-BP100 or RW-BP100 to 500 μM of POPC/POPG (1:1 molar) vesicles, or 50 μM of BP100 to POPC or POPC/POPG (4:1 molar) vesicles. The OD values were normalized for the baseline. No aggregation and, therefore, no increase in OD was observed for POPC or POPC/POPG (4:1) vesicles. The three peptides induce aggregation of POPC/POPG (1:1) vesicles. (D) Kinetics of vesicle leakage induced by 25 μM of BP100, R-BP100 and RW-BP100 in the presence of 50 μM POPC/POPG (1:1 molar) and POPC vesicles, as followed by dequenching of CF. The fluorescence signal was converted into % of leakage; TX-100 0.1% (v/v) was added at the end of each kinetics (not shown) to establish 100% of leakage in each assay.

Table 2
Vesicle leakage induced by BP100, R-BP100 and RW-BP100.[a]

Peptide	Lipid mixture	$LC_{50} \pm SE$ (μM) [b]	$T_{1/2} \pm SE$ (s)[c]
BP100	POPC	>100	6.21 ± 0.30
	POPC/POPG (1:1)	3.71 ± 0.11	4.85 ± 0.04
R-BP100	POPC	83.28 ± 8.89	3.67 ± 0.23
	POPC/POPG (1:1)	5.06 ± 1.66	0.37 ± 0.04
RW-BP100	POPC	10.71 ± 0.67	0.63 ± 0.07
	POPC/POPG (1:1)	5.16 ± 0.34	0.14 ± 0.01

[a]Peptides were incubated with vesicles suspensions containing 50 μM of total lipid concentration. [b]The peptide concentration needed to achieve 50% leakage (LC50) and the standard errors were determined by fitting a non-linear regression equation in which the maximum response was fixed to 100% leakage. [c]Time required to achieve half of the maximum response upon addition of 25 μM of peptide to lipid suspension containing 50 μM of lipid.

Trp residue more deeply inserted in the membrane, than the Tyr in R-BP100 or in BP100 peptide.

3.9. Membrane in-depth location of BP100 and its analogues

The location of the Tyr/Trp residue when the peptides are bound to the membrane was monitored by a differential quenching approach. 5- and 16-NS are stearic acid molecules derivatized (carbon 5 or 16) with a doxyl group, a quencher of the Tyr and Trp fluorescence. With a differential depth location in the membrane, the doxyl group in 5-NS more efficiently quenches fluorophores located in the water_membrane interface, whereas 16-NS is more efficient as a quencher of fluorophores more deeply inserted [33]. In addition, acrylamide, a soluble quencher unable to partition extensively into lipidic membranes, was used to quench fluorophores accessible to the aqueous environment [31] and its quenching efficiency was measured in the absence and presence of LUVs suspension.

The relative quenching efficiency can be compared with the Stern–Volmer constant, K_{SV} (Table 4). All of the peptides tested were more efficiently quenched by acrylamide in the absence of model membranes than in their presence, suggesting that the peptides are inserted into the lipid bilayer and less accessible to the aqueous environment. In addition, the fluorescence of all the peptides is more efficiently quenched in the presence of POPC/POPG (1:1 molar) relative to POPC model membranes, which confirms better insertion into negatively-charged than into zwitterionic membranes.

In POPC membranes all of the peptides have the fluorescent residue more accessible to 5-NS than to 16-NS, suggesting a location in the interface. In POPC/POPG (1:1) membranes, RW-BP100 is more efficiently quenched by 16-NS than 5-NS, suggesting a deeper insertion, whereas the fluorescence of BP100 or R-BP100 is quenched by 5- and 16-NS with identical efficiency. A deeper insertion of RW-BP100 into POPC/POPG (1:1) membrane is consistent with the larger change in the dipolar potential (see Fig. 6B) and lower surface destabilization observed by aggregation studies, when compared with the other two analogues (see Fig. 6C). Altogether these results show that the Tyr/Trp region of the molecule can insert in the hydrophobic region of the phospholipid membrane.

Table 3
Affinity of BP100, R-BP100 and RW-BP100 for different lipid mixtures.[a]

Peptide	Lipid mixture	K_p ($\times 10^3$)	I_L/I_W
BP100	POPC	0.26 ± 0.9	2.11 ± 1.86
	POPC/POPG (4:1)	1.19 ± 0.17	2.12 ± 0.67
	POPC/POPG (1:1)	3.97 ± 1.05	2.27 ± 1.27
R-BP100	POPC	1.51 ± 0.11	2.51 ± 0.42
	POPC/POPG (4:1)	3.54 ± 0.36	2.86 ± 0.62
	POPC/POPG (1:1)	6.26 ± 0.96	2.72 ± 0.88
RW-BP100	POPC	1.12 ± 0.06	4.30 ± 0.59
	POPC/POPG (4:1)	3.09 ± 0.56	3.98 ± 1.62
	POPC/POPG (1:1)	27.9 ± 7.90	3.41 ± 1.99

[a] Peptides were titrated with LUV suspensions and the fluorescence emission signal (I/I_W) plotted as a function of lipid concentration. The Kp and I_L/I_W parameters were obtained from fitting a non-linear equation.

Table 4
Emission fluorescence quenching of BP100, R-BP100 and RW-BP100 induced by 5-NS, 16-NS or acrylamide.[a]

Peptide	Lipid mixture	$K_{SV,\ 5\text{-}NS}$ (M^{-1})	$K_{SV,\ 16\text{-}NS}$ (M^{-1})	$K_{SV,\ acrylamide}$ (M^{-1})
BP100	POPC	0.80 ± 0.16	0.55 ± 0.23	9.60 ± 0.82
	POPC/POPG (1:1)	2.47 ± 0.06	2.02 ± 0.06	1.94 ± 0.29
	Buffer			34.10 ± 1.57
R-BP100	POPC	1.36 ± 2.10[b]	0.21 ± 0.22	4.88 ± 0.30
	POPC/POPG (1:1)	1.88 ± 0.09	1.72 ± 0.15	1.37 ± 0.26
	Buffer			8.80 ± 0.22
RW-BP100	POPC	7.48 ± 1.47	2.86 ± 0.34	4.79 ± 0.34
	POPC/POPG (1:1)	0.68 ± 0.24	2.19 ± 0.27	3.23 ± 0.21
	Buffer			18.40 ± 0.63

[a]Each peptide was titrated with a quenching agent (5-NS, 16-NS or acrylamide) in the presence or absence of LUVs and quantified by Stern–Volmer constant, K_{SV}. K_{SV} and standard errors were determined by fitting the Stern–Volmer equation. [b]Stern–Volmer representation shows a positive deviation, therefore K_{SV} was determined by fitting a quenching with sphere-of-action.

3.10. CD spectroscopy in the presence of membrane vesicles

To analyse the structure of the peptides in aqueous solution and in the presence of lipid membrane we performed CD measurements (Fig. 7). In buffer all peptides had very low ellipticity above 210 nm and a strong negative band near 195 nm, which is typical of a random coil structure [45]. A lack of structure was confirmed in the presence of urea, a denaturizing agent. No alterations in CD signals were detected for any of the peptides, even with concentrations as high as 5 M urea (data not shown). In addition, all the peptides maintained a random coil conformation in buffer with pH 2 (data not shown).

In the presence of anionic vesicles the three peptides show a transition from unstructured to helical form, revealing a change in conformation upon membrane insertion. With POPC no alterations in the CD signal were detected, suggesting the requirement of anionic phospholipids for an alteration in the conformation. A helical wheel conformation suggests an amphipathic structure with the nonpolar residues in one side and the positive side chains in the other face of the helix.

4. Discussion

In this study we designed two new AMPs, R-BP100 and RW-BP100, and compared their antimicrobial activities and toxic properties with the parent analogue BP100. Atomic force microscopy with bacterial cells and biophysical studies with model membranes were employed to gain insights on the mechanism of action of BP100 and its analogues.

MIC and MBC assays revealed that the newly designed AMPs are more active than BP100, previously reported to be active against Gram-negative bacteria [14] but inactive against the Gram-positive *S. aureus* [17]. Here we show that R-BP100 and RW-BP100 were not only active against Gram-negative bacteria, but also had activity against Gram-positive bacteria at low micromolar concentrations (see Table 1). Although RW-BP100 is the most toxic analogue, it has the highest TI against the tested Gram-negative bacteria. To decrease the toxic properties without compromising the amphipathic character, shifting the position of the Trp residue within the hydrophobic part of the amphipathic helix is a possibility [46].

AFM imaging suggests that BP100, R-BP100 and RW-BP100 exert their action by targeting the anionic bacterial surface and disrupting the membrane integrity. A mechanism dependent on electrostatic attractions between the polycationic peptides and the anionic microbial surface, followed by insertion into and permeabilization of the cytoplasmic membrane, is supported by biophysical results obtained with

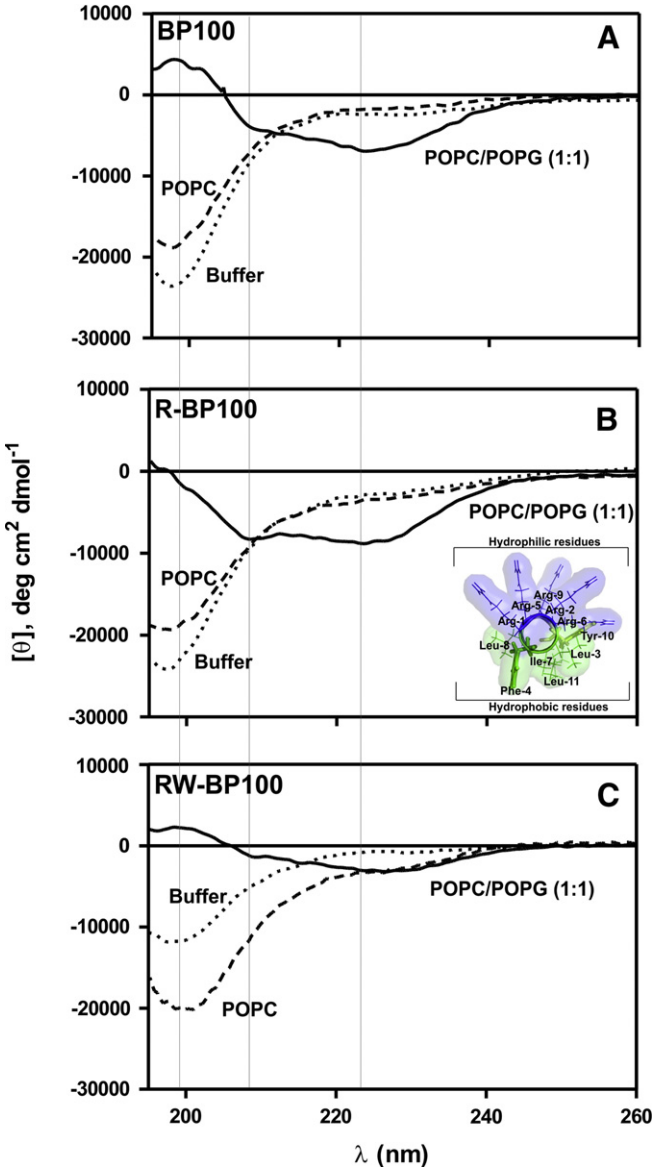

Fig. 7. CD spectra of BP100 and its analogues in the absence or presence of lipid vesicles. CD spectra of 50 μM of BP100 (A), R-BP100 (B) and RW-BP100 (C) in 10 mM phosphate buffer containing 150 mM NaF or in the presence of POPC (500 μM) or in the presence of POPC/POPG (1:1) (500 μM for R-BP100 and RW-BP100 and 1 mM for BP100). Insert in panel B shows the top view of predicted helical three-dimensional structure of R-BP100 in anionic membrane environment putting in evidence the amphipathic character of the helix. Hydrophilic amino acid residues are coloured in blue, hydrophobic amino acids are coloured in green. The side chains of Phe and Tyr residues are represented by ball and stick. The image was modulated using PyMOL Molecular Graphics System, version 1.2r3pre (Schrödinger, LLC).

model membranes (see Figs. 4–7). Our studies revealed that the peptides in this study are able to bind and neutralize both LTA and LPS, the negatively-charged molecules exposed at the Gram-negative and Gram-positive bacteria, respectively. Furthermore, SPR and fluorescence studies revealed that the peptides are able to bind and insert into lipid bilayers, preferring anionic over neutral membranes. Upon insertion into anionic membranes, the three peptides acquire an amphipathic helical conformation (see Fig. 7B), insert into the lipid bilayer, as confirmed with the fluorescence properties of the Tyr/Trp residue (see Tables 3 and 4), and promote local perturbations, as revealed by changes in the dipolar potential and vesicle aggregation (see Fig. 6). The amphipathic helical conformation maximizes both electrostatic and hydrophobic interactions with the membrane as the positive face promotes binding to the anionic headgroups, whereas the nonpolar face favours contact with the hydrophobic part of the membrane [47] and allows insertion of the molecule into the hydrophobic core of the lipid bilayer [11]. As a result of binding, insertion and accumulation into the phospholipid bilayer, BP100 and its analogues induce membrane disturbances that result in membrane permeabilization (see Fig. 6D).

A mechanism of action dependent on binding to the anionic bacterial surface, followed by peptide insertion into the membrane, and permeabilization is in agreement with previous studies with BP100 [15,17]. Biophysical studies with model membranes and *E. coli* cells revealed that BP100 binds to the anionic surface of *E. coli* cells, inserts into the phospholipid bilayer and induces the leakage of cytoplasmic content from *E. coli* cells [17].

Electrostatic interactions and amphipathic structure are clearly important for the activity of BP100, and its analogues, but they cannot explain the differences in the relative efficiency of the three peptides against Gram-positive bacteria. All the tested peptides acquire a helical amphipathic structure upon interaction with negatively-charged membranes, have identical ability to induce leakage from negatively-charged membranes, have the same global net charge (+6) and are able to bind to LTA, but BP100 has weak activity against Gram-positive bacteria, whereas R-BP100 and RW-BP100 are active. The activity of the three analogues against Gram-positive bacteria tracks with their membrane-binding affinity. Even with the same charge and preference for anionic membranes, R-BP100 and RW-BP100, are better adapted to establish interactions with membranes, than BP100. The preference of these newly designed peptides for the membrane environment is in agreement with their higher overall hydrophobicity, but might also be the result of particular features of the Arg and Trp residues.

The higher membrane-binding affinity of R-BP100 over BP100 results from the substitution of the Lys residues with Arg. Although Lys and Arg have the same charge, their membrane-binding properties are different, suggesting that not only the charge but some specific properties of the guanidinium side chain in Arg are responsible for this behaviour [48]. One possible explanation is the pronounced ability of the guanidinium group to establish strong bidentate H-bonds with phosphate moieties from two lipid headgroups, whereas the Lys ammonium side chain can only interact with a single lipid headgroup (Fig. 8A & B) [49]. In addition of being better H-bond donors, guanidinium side chains also establish stronger electrostatic cation–π interactions with aromatic residues, than Lys residues [50]. Cation–π interactions occur between basic residues (Arg and Lys) and aromatic residues (Phe, Tyr and Trp) [50] and are important for peptide self-association within membranes and facilitate deeper insertion into membranes by shielding cationic side chains [50,51]. Furthermore, the Arg side chain is able to form H-bonds even when involved in cation–π interactions, whereas the Lys side chain cannot [52].

RW-BP100, besides having the Lys mutated with Arg, also possesses a Trp instead of a Tyr residue, which confers higher affinity and deeper insertion into the membrane relative to the analogue R-BP100 (see Fig. 6 and Table 4). These results are in agreement with previous studies showing that the Trp residue not only partitions more favourably in the membrane interface, but is also more hydrophobic and has higher affinity for bulk hydrophobic phases, than Tyr [38]. In addition, the Trp residue facilitates the insertion of the cationic Arg into the membrane hydrophobic region through cation–π interactions [19] as above mentioned. The importance of Trp residues on the antimicrobial activity of peptides has been previously correlated with their ability to bind to lipid membranes [18,19,53] and is further supported in this study.

Based on our findings we propose that to efficiently kill Gram-positive bacteria by a membrane-dependent mechanism a peptide should be able to: target anionic membranes through electrostatic interactions; partition into the water–lipid interface regions of membranes through hydrophobic interactions and H-bonds; and be able to more deeply insert into the hydrophobic membrane environment,

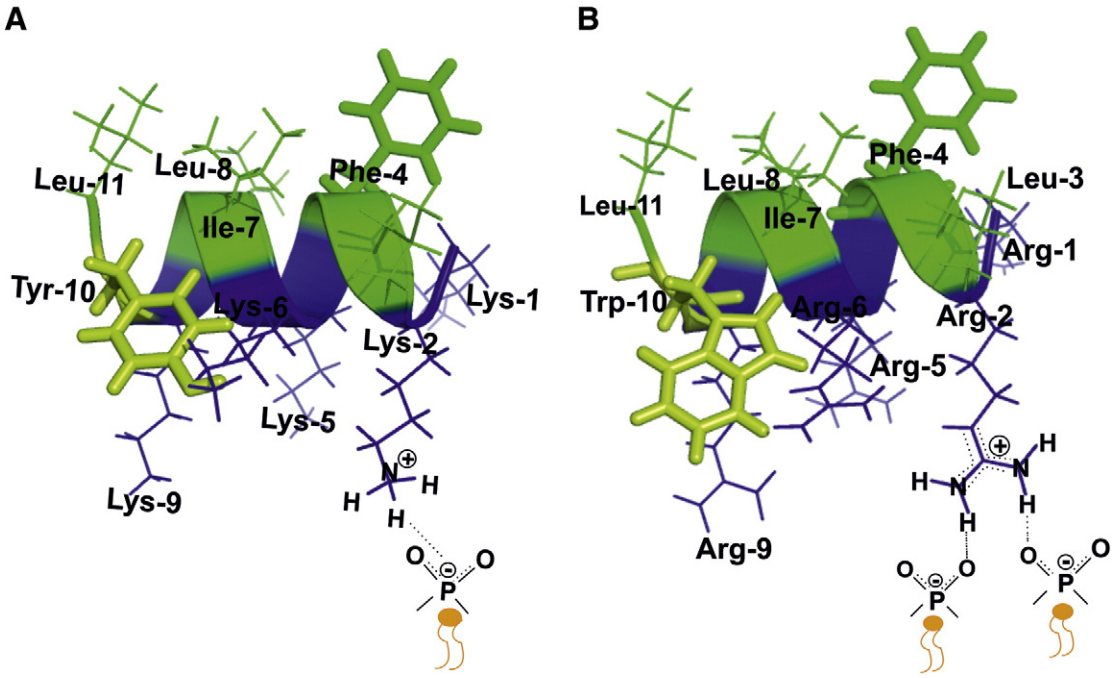

Fig. 8. Representation of the predicted helical three-dimensional structure of BP100 and its analogues in anionic membrane environment. (A) Side view of BP100 showing the ability of Lys residues to establish monodentate H-bonds. (B) Side view of RW-BP100 showing the ability of Arg residues to establish bidentate H-bonds with phosphate groups from two different phospholipids. The colour scheme is the same as in Fig. 7B; the two images were modulated using PyMOL Molecular Graphics System, version 1.2r3pre (Schrödinger, LLC).

where the ability to establish cation–π interactions seems to be important to shield the charge of the cationic residues and disrupt the phospholipid membrane.

The three peptides are highly active against the tested Gram-negative bacteria, showing that these bacteria can be targeted and disrupted by peptides containing either Arg or Lys residues. We propose that to kill Gram-negative bacteria, H-bond formation and cation–π interactions are not as important as for Gram-positive bacteria. The Gram-negative bacterial surface is covered with LPS molecules, which form a very compact and impermeable layer due to non-covalent associations with divalent (calcium and magnesium) cations [54]; the activity of cationic peptides against Gram-negative bacteria has been correlated with their ability to bind and cross the LPS barrier by displacing divalent cations from their binding sites [1,41,54] and eventually disrupting the cytoplasmic membrane. A mechanism of action dependent on binding and crossing the LPS barrier before disrupting the inner membrane is consistent with the *E. coli* strain CGSC 5167 (with rough LPS, and therefore more penetrable) being more susceptible to all the peptides, than the control strain ATCC 25922 (with smooth LPS) (see Table 1). The importance of Arg and Trp residues for activity against Gram-positive, but not Gram-negative bacteria, could be the result of a larger peptidoglycan layer in the Gram-positive outer membrane, relative to Gram-negative bacteria, which requires the unique hydrogen binding geometry of Arg and is facilitated by the complex amphipathic properties of Trp that together promote stable and deep insertion into the cell wall of Gram-positive bacteria.

5. Conclusions

In this study we designed two BP100 analogues, which in addition to being active against the tested Gram-negative were also active against Gram-positive bacteria. Identification of peptides with high activity against Gram-negative and Gram-positive bacteria is of major relevance due to the development of strains with resistance to common antibiotics. In fact, the novel peptides were here shown to be active against several pathogenic bacteria, including strains with antibiotic resistance.

Our studies revealed that whereas the antimicrobial activity of BP100 and its analogues against Gram-negative bacteria seems to be mainly dependent on an ability to bind to LPS layer through electrostatic interactions and membrane disruption through hydrophobic interactions. The activity against Gram-positive, although dependent on electrostatic attractions, and phospholipid membrane disruption, requires further interactions with the cell wall components in which H-bonds and cation–π interactions might play a role. Overall, the results obtained in this study provide valuable information on the correlation between amino acid sequence and antimicrobial activity that can guide the development of new AMPs with either specific activity or a broader spectrum of action.

Acknowledgements

IMT work was supported by a grant (PTDC/SAU-BEB/099142/2008), HGF and DG held a scholarship from the Fundação para a Ciência e Tecnologia, Portugal, SFRH/BD/39039/2007 and SFRH/BPD/73500/2010, respectively. STH is the recipient of a Discovery Early Career Researcher Award (DE120103152), awarded by Australian Research Council. DJC is a National Health and Medical Research Council Fellow. We thank Marta Ribeiro (IMM, Lisbon University) for the valuable scientific discussions. We thank Dr Mark Blaskovich (IMB, UQ) for kindly providing the bacterial strains employed in this study and Angela Kavanagh (IMB, UQ) for the help in establishing the antimicrobial assays.

References

[1] M. Zasloff, Antimicrobial peptides of multicellular organisms, Nature 415 (2002) 389–395.
[2] M.L. Mangoni, Y. Shai, Short native antimicrobial peptides and engineered ultrashort lipopeptides: similarities and differences in cell specificities and modes of action, Cell Mol. Life Sci. 68 (2011) 2267–2280.
[3] M. Pasupuleti, A. Schmidtchen, M. Malmsten, Antimicrobial peptides: key components of the innate immune system, Crit. Rev. Biotechnol. 32 (2012) 143–171.
[4] M.L. Mangoni, Y. Shai, Temporins and their synergism against Gram-negative bacteria and in lipopolysaccharide detoxification, Biochim. Biophys. Acta 1788 (2009) 1610–1619.

[5] W.C. Wimley, Describing the mechanism of antimicrobial peptide action with the interfacial activity model, ACS Chem. Biol. 5 (2010) 905–917.
[6] M.R. Yeaman, N.Y. Yount, Mechanisms of antimicrobial peptide action and resistance, Pharmacol. Rev. 55 (2003) 27–55.
[7] K. Matsuzaki, K. Sugishita, M. Harada, N. Fujii, K. Miyajima, Interactions of an antimicrobial peptide, magainin 2, with outer and inner membranes of Gram-negative bacteria, Biochim. Biophys. Acta 1327 (1997) 119–130.
[8] R. Bessalle, H. Haas, A. Goria, I. Shalit, M. Fridkin, Augmentation of the antibacterial activity of magainin by positive-charge chain extension, Antimicrob. Agents Chemother. 36 (1992) 313–317.
[9] M. Dathe, H. Nikolenko, J. Meyer, M. Beyermann, M. Bienert, Optimization of the antimicrobial activity of magainin peptides by modification of charge, FEBS Lett. 501 (2001) 146–150.
[10] C. Friedrich, M.G. Scott, N. Karunaratne, H. Yan, R.E. Hancock, Salt-resistant alpha-helical cationic antimicrobial peptides, Antimicrob. Agents Chemother. 43 (1999) 1542–1548.
[11] I. Zelezetsky, A. Tossi, Alpha-helical antimicrobial peptides—using a sequence template to guide structure–activity relationship studies, Biochim. Biophys. Acta 1758 (2006) 1436–1449.
[12] C.B. Park, K.S. Yi, K. Matsuzaki, M.S. Kim, S.C. Kim, Structure–activity analysis of buforin II, a histone H2A-derived antimicrobial peptide: the proline hinge is responsible for the cell-penetrating ability of buforin II, Proc. Natl. Acad. Sci. U.S.A. 97 (2000) 8245–8250.
[13] M. Cudic, L. Otvos Jr., Intracellular targets of antibacterial peptides, Curr. Drug Targets 3 (2002) 101–106.
[14] E. Badosa, R. Ferre, M. Planas, L. Feliu, E. Besalu, J. Cabrefiga, E. Bardaji, E. Montesinos, A library of linear undecapeptides with bactericidal activity against phytopathogenic bacteria, Peptides 28 (2007) 2276–2285.
[15] R. Ferre, M.N. Melo, A.D. Correia, L. Feliu, E. Bardaji, M. Planas, M. Castanho, Synergistic effects of the membrane actions of cecropin-melittin antimicrobial hybrid peptide BP100, Biophys. J. 96 (2009) 1815–1827.
[16] K. Eggenberger, C. Mink, P. Wadhwani, A.S. Ulrich, P. Nick, Using the peptide BP100 as a cell-penetrating tool for the chemical engineering of actin filaments within living plant cells, Chembiochem 12 (2011) 132–137.
[17] C.S. Alves, M.N. Melo, H.G. Franquelim, R. Ferre, M. Planas, L. Feliu, E. Bardaji, W. Kowalczyk, D. Andreu, N.C. Santos, M.X. Fernandes, M.A. Castanho, Escherichia coli cell surface perturbation and disruption induced by antimicrobial peptides BP100 and pepR, J. Biol. Chem. 285 (2010) 27536–27544.
[18] K. Hilpert, R. Volkmer-Engert, T. Walter, R.E. Hancock, High-throughput generation of small antibacterial peptides with improved activity, Nat. Biotechnol. 23 (2005) 1008–1012.
[19] D.I. Chan, E.J. Prenner, H.J. Vogel, Tryptophan- and arginine-rich antimicrobial peptides: structures and mechanisms of action, Biochim. Biophys. Acta 1758 (2006) 1184–1202.
[20] Y.B. Huang, X.F. Wang, H.Y. Wang, Y. Liu, Y. Chen, Studies on mechanism of action of anticancer peptides by modulation of hydrophobicity within a defined structural framework, Mol. Cancer Ther. 10 (2011) 416–426.
[21] I. Wiegand, K. Hilpert, R.E. Hancock, Agar and broth dilution methods to determine the minimal inhibitory concentration (MIC) of antimicrobial substances, Nat. Protoc. 3 (2008) 163–175.
[22] P. Eaton, J.C. Fernandes, E. Pereira, M.E. Pintado, F. Xavier Malcata, Atomic force microscopy study of the antibacterial effects of chitosans on Escherichia coli and Staphylococcus aureus, Ultramicroscopy 108 (2008) 1128–1134.
[23] B. Fang, S. Gon, M. Park, K.N. Kumar, V.M. Rotello, K. Nusslein, M.M. Santore, Bacterial adhesion on hybrid cationic nanoparticle-polymer brush surfaces: ionic strength tunes capture from monovalent to multivalent binding, Colloids Surf. B: Biointerfaces 87 (2011) 109–115.
[24] Y.H. Huang, M.L. Colgrave, R.J. Clark, A.C. Kotze, D.J. Craik, Lysine-scanning mutagenesis reveals an amendable face of the cyclotide kalata B1 for the optimization of nematocidal activity, J. Biol. Chem. 285 (2010) 10797–10805.
[25] Z. Zidek, E. Kmonickova, P. Kostecka, P. Jansa, Microfiltration method of removal of bacterial contaminants and their monitoring by nitric oxide and Limulus assays, Nitric Oxide 28C (2012) 1–7.
[26] S.T. Henriques, M.A. Castanho, Consequences of nonlytic membrane perturbation to the translocation of the cell penetrating peptide pep-1 in lipidic vesicles, Biochemistry 43 (2004) 9716–9724.
[27] S.T. Henriques, L.K. Pattenden, M.I. Aguilar, M.A. Castanho, PrP(106–126) does not interact with membranes under physiological conditions, Biophys. J. 95 (2008) 1877–1889.
[28] S.T. Henriques, M.A. Castanho, L.K. Pattenden, M.I. Aguilar, Fast membrane association is a crucial factor in the peptide pep-1 translocation mechanism: a kinetic study followed by surface plasmon resonance, Biopolymers 94 (2010) 314–322.
[29] P.M. Matos, M.A. Castanho, N.C. Santos, HIV-1 fusion inhibitor peptides enfuvirtide and T-1249 interact with erythrocyte and lymphocyte membranes, PLoS One 5 (2010) e9830.
[30] Y.H. Huang, M.L. Colgrave, N.L. Daly, A. Keleshian, B. Martinac, D.J. Craik, The biological activity of the prototypic cyclotide kalata b1 is modulated by the formation of multimeric pores, J. Biol. Chem. 284 (2009) 20699–20707.
[31] S.T. Henriques, M.A. Castanho, Environmental factors that enhance the action of the cell penetrating peptide pep-1 A spectroscopic study using lipidic vesicles, Biochim. Biophys. Acta 1669 (2005) 75–86.
[32] N.C. Santos, M. Prieto, M.A.R.B. Castanho, Quantifying molecular partition into model systems of biomembranes: an emphasis on optical spectroscopic methods, Biochim. Biophys. Acta 1612 (2003) 123–135.
[33] M.X. Fernandes, J. Garcia de la Torre, M.A. Castanho, Joint determination by Brownian dynamics and fluorescence quenching of the in-depth location profile of biomolecules in membranes, Anal. Biochem. 307 (2002) 1–12.
[34] M.A. Castanho, M.J. Prieto, Fluorescence quenching data interpretation in biological systems. The use of microscopic models for data analysis and interpretation of complex systems, Biochim. Biophys. Acta 1373 (1998) 1–16.
[35] Y. Shai, Mode of action of membrane active antimicrobial peptides, Biopolymers 66 (2002) 236–248.
[36] W.C. Wimley, S.H. White, Experimentally determined hydrophobicity scale for proteins at membrane interfaces, Nat. Struct. Biol. 3 (1996) 842–848.
[37] J.L. MacCallum, D.P. Tieleman, Hydrophobicity scales: a thermodynamic looking glass into lipid-protein interactions, Trends Biochem. Sci. 36 (2011) 653–662.
[38] S.H. White, W.C. Wimley, Hydrophobic interactions of peptides with membrane interfaces, Biochim. Biophys. Acta 1376 (1998) 339–352.
[39] M.N. Melo, R. Ferre, L. Feliu, E. Bardaji, M. Planas, M.A. Castanho, Prediction of antibacterial activity from physicochemical properties of antimicrobial peptides, PLoS One 6 (2011) e28549.
[40] T.J. Silhavy, D. Kahne, S. Walker, The bacterial cell envelope, Cold Spring Harb. Perspect. Biol. 2 (2010) a000414.
[41] Y. Rosenfeld, Y. Shai, Lipopolysaccharide (Endotoxin)-host defense antibacterial peptides interactions: role in bacterial resistance and prevention of sepsis, Biochim. Biophys. Acta 1758 (2006) 1513–1522.
[42] P.M. Matos, H.G. Franquelim, M.A. Castanho, N.C. Santos, Quantitative assessment of peptide-lipid interactions. Ubiquitous fluorescence methodologies, Biochim. Biophys. Acta 1798 (2010) 1999–2012.
[43] A. Mulgrew-Nesbitt, K. Diraviyam, J. Wang, S. Singh, P. Murray, Z. Li, L. Rogers, N. Mirkovic, D. Murray, The role of electrostatics in protein-membrane interactions, Biochim. Biophys. Acta 1761 (2006) 812–826.
[44] N.C. Santos, M.A.R.B. Castanho, Fluorescence spectroscopy methodologies on the study of proteins and peptides. On the 150th anniversary of protein fluorescence, Trends Appl. Spectrosc. 4 (2002) 113–125.
[45] N.J. Greenfield, Using circular dichroism spectra to estimate protein secondary structure, Nat. Protoc. 1 (2006) 2876–2890.
[46] O. Rekdal, B.E. Haug, M. Kalaaji, H.N. Hunter, I. Lindin, I. Israelsson, T. Solstad, N. Yang, M. Brandl, D. Mantzilas, H.J. Vogel, Relative spatial positions of tryptophan and cationic residues in helical membrane-active peptides determine their cytotoxicity, J. Biol. Chem. 287 (2012) 233–244.
[47] J. Seelig, Thermodynamics of lipid-peptide interactions, Biochim. Biophys. Acta 1666 (2004) 40–50.
[48] Y. Su, T. Doherty, A.J. Waring, P. Ruchala, M. Hong, Roles of arginine and lysine residues in the translocation of a cell-penetrating peptide from (13)C, (31)P, and (19)F solid-state NMR, Biochemistry 48 (2009) 4587–4595.
[49] J.B. Rothbard, T.C. Jessop, P.A. Wender, Adaptive translocation: the role of hydrogen bonding and membrane potential in the uptake of guanidinium-rich transporters into cells, Adv. Drug Deliv. Rev. 57 (2005) 495–504.
[50] J.P. Gallivan, D.A. Dougherty, Cation-pi interactions in structural biology, Proc. Natl. Acad. Sci. U. S. A. 96 (1999) 9459–9464.
[51] S. Mecozzi, A.P. West Jr., D.A. Dougherty, Cation-pi interactions in aromatics of biological and medicinal interest: electrostatic potential surfaces as a useful qualitative guide, Proc. Natl. Acad. Sci. U. S. A. 93 (1996) 10566–10571.
[52] M.P. Aliste, J.L. MacCallum, D.P. Tieleman, Molecular dynamics simulations of pentapeptides at interfaces: salt bridge and cation-pi interactions, Biochemistry 42 (2003) 8976–8987.
[53] A.A. Stromstedt, M. Pasupuleti, A. Schmidtchen, M. Malmsten, Evaluation of strategies for improving proteolytic resistance of antimicrobial peptides by using variants of EFK17, an internal segment of LL-37, Antimicrob. Agents Chemother. 53 (2009) 593–602.
[54] L. Leive, The barrier function of the gram-negative envelope, Ann. N. Y. Acad. Sci. 235 (1974) 109–129.